Background-oriented schlieren technique for two-dimensional visualization of convective indoor air flows

Lia Becher, Conrad Voelker, Volker Rodehorst, Michael Kuhne

Bauhaus University Weimar, Department of Building Physics
Coudraystrasse 11A
99423 Weimar, Germany
Email: lia.becher@uni-weimar.de

(Received 4 February 2020; Revised 28 April 2020; Accepted 14 June 2020)

Abstract

This article focuses on further developments of the background-oriented schlieren (BOS) technique to visualize convective indoor air flow, which is usually defined by very small density gradients. Since the light rays deflect when passing through fluids with different densities, BOS can detect the resulting refractive index gradients as integration along a line of sight. In this paper, the BOS technique is used to yield a two-dimensional visualization of small density gradients. The novelty of the described method is the implementation of a highly sensitive BOS setup to visualize the ascending thermal plume from a heated thermal manikin with temperature differences of minimum 1 K. To guarantee steady boundary conditions, the thermal manikin was seated in a climate laboratory. For the experimental investigations, a high-resolution DLSR camera was used capturing a large field of view with sufficient detail accuracy. Several parameters such as various backgrounds, focal lengths, room air temperatures, and distances between the object of investigation, camera, and structured background were tested to find the most suitable parameters to visualize convective indoor air flow. Besides these measurements, this paper presents the analyzing method using cross-correlation algorithms and finally the results of visualizing the convective indoor air flow with BOS. The highly sensitive BOS setup presented in this article complements the commonly used invasive methods that highly influence weak air flows.

1. Introduction

It is common to use anemometers to measure the indoor air flow or temperature sensors, e.g. thermally sensitive resistors with negative temperature coefficient (NTC thermistors), to measure the air temperature. However, these instruments measure the flow field only at a specific location and generally hamper the flow, some also emit heat. This can cause errors, especially when investigating slow convective air flow. Alternative techniques, like particle image velocimetry (PIV) or particle streak tracking (PST), use particles to depict the flow. Hereby, the considerable effort during the measurement process and potential measurement errors, e.g. following behavior of the particles, are disadvantageous. To investigate flow without disturbing particles, schlieren imaging with the help of a schlieren mirror can be used. This technique is highly sensitive to capturing density gradients. However, the range of measurement is constrained due to the limited size of the mirror required, restricting the implementation to investigate indoor air flows. Both schlieren imaging and PST, as well as anemometry and temperature sensors have been used by the authors to study transient indoor air flows (Gena et al. 2020; Voelker et al. 2014). Due to their invasive properties and the spatial restrictions of the schlieren mirror, the optical BOS technique was introduced to investigate large-scale indoor air flows without any disturbances.

BOS visualizes flow either two-dimensionally or three-dimensionally with stereoscopic or tomographic measurement setups. BOS is able to depict differences in densities of fluids due to differences in temperature or pressure. For light rays, these density gradients cause refractive index gradients that can be detected by BOS. Snell's law states that refractive index gradients are visible due to the light slowing down when passing through substances. If the medium is homogeneous, such as a vacuum, light travels at a constant speed. If it reaches a medium with a different density, light rays will change their speed and therefore become deflected to the extent defined by the density gradient. The result is discontinuous movement, which occurs in a schliere[1] (Mazumdar 2013).

To capture the schlieren, the object of interest, which causes the density gradient (phase object), is placed in front of a structured background. A camera records the virtual displacement of the background, which occurs due to phase object. The recorded light rays are integrated along a line of sight for a three-dimensional flow field imaged on a two-dimensional plane. When using several cameras, the flow field can be reconstructed three-dimensionally using stereoscopic or tomographic algorithms.

Currently, BOS is successfully used in numerous fields, e.g. aerodynamics and shock waves. Due to the technique's continuous development over the past few years, many modified BOS systems have emerged. By varying certain parameters, BOS can adapt to various boundary conditions to optimize the imaging of the density gradients. Raffel (2015) gives a good overview about the different BOS techniques that are commonly used to visualize air flows two- or three-dimensionally. Further work is done by Hargather and Settles (2012) who report that the sensitivity of a BOS system is nearly equal to that of the schlieren technique using a schlieren mirror as mentioned earlier. Furthermore, several approaches show that BOS can be combined with other techniques, e.g. BOS velocimetry (Settles 2010), diffractive optical element based BOS (Rajshekhar and Ambrosini 2018; Ramaiah et al. 2020), or reference-free digital shadowgraphy using a moving BOS background (Gardner et al. 2020). The accuracy of BOS has been analyzed and optimized showing that the dynamic range is approximately 50:1; measurement errors amount to 2-3 % in full range (Raffel 2015).

So far, BOS only has been used to visualize density gradients that result from rather large differences in temperature or pressure of the fluid. Therefore, a BOS setup has been developed that tries to outbid the sensitivity of the measurements to investigate convective indoor air flows.

2. Experiments and methodology

2.1. The concept of BOS

The principle of schlieren is similar to the observation of heat shimmer or fata morganas when density changes between the human eye and a distant object lead to distortions or even reflections (Goldhahn 2009). The term *background-oriented* means that the camera focuses exclusively on the background behind the phase object under investigation (refractive index gradient). Hence, the phase object does not appear sharply but refracts the rays reflected by the background. The BOS system is not restricted to spatial dimensions and can be adjusted appropriately to precisely record the flow field under investigation.

The setup of the BOS system consists of a structured background with a randomly distributed dot pattern, a camera that records the measuring field, and the phase object, see Fig. 1. To evaluate the density gradients, a measuring image with the phase object (flow-on) is taken first. Subsequently, a reference image is taken that only shows the background without the disturbing flow (flow-off). When these two images are compared, a certain pixel on the reference image appears at a different place (image shift Δy at the image plane). This is due to the linear relation between the gas density ρ and the refractive index n for air and most other gases, described by the Gladstone-Dale equation

[1] A *schliere* (German, singular) describes disturbances in inhomogeneous transparent media. *Schlieren* (plural) appear as relatively small diffraction differences and deflect light rays in any direction other than the direction z of the medium (Settles 2001).

$$n - 1 = k\rho \quad (1)$$

with the Gladstone-Dale coefficient $k \approx 2{,}3\text{E-}4\ m^3/kg$. It states that density gradients cause refractive index gradients. Light rays that pass through a test area are deflected to the same extent as the density gradient allows it (Panigrahi and Muralidhar 2012).

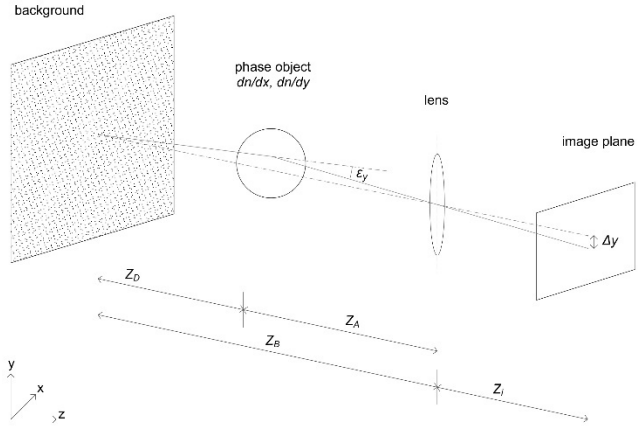

Fig. 1 *Schematic setup of the BOS system (modified from Raffel et al. (2018))*

The light deflection resulting in the virtual displacement Δy is described by the deflection angle ε_y. Assuming parallel light rays in Gaussian optics and small deflection angles: $\tan \varepsilon_y \approx \varepsilon_y$. Eqn. 2 states that high image shifting Δy can be achieved by a large distance Z_D.

$$\Delta y = Z_D \frac{Z_i}{Z_B} \varepsilon_y \quad (2)$$

The deflection angle ε_y is defined by

$$\varepsilon_y = \frac{1}{n_0} \int \frac{\delta_n}{\delta_y} dz \quad (3)$$

and the distance from the lens to the image plane by

$$Z_i = \frac{f\ Z_B}{Z_B - f} \quad (4)$$

Here, n is the refractive index of the gradient, n_0 is the reference refractive index of the indoor air, and f is the focal length (Raffel 2015).

Using the adapted thin-lens approximation (Keagy and Ellis 1948)

$$\varepsilon_y = 2(\frac{n}{n_0} - 1) \quad (5)$$

it is possible to roughly estimate the refraction angle ε_y, which is in radians and then converted to arcseconds by multiplying it by 206265 (Settles 2001). Using Eqn. 2, the approximate pixel shift Δy then can be calculated.

The maximum image shift for an increasing distance Z_D approximates $y = f\ \varepsilon_y$ (Raffel et al. 2018). However, Z_A needs to be large enough to achieve sufficiently sharp measuring images. The phase object appears more blurred when Z_A decreases due to the camera focusing only on the background. This conflict can be minimized while keeping the aperture as small as possible to maintain the depth of field.

Furthermore, the sensitivity of the setup will not change if the ratio Z_A / Z_B stays the same. Rather, the camera's resolution is to be increased as well as the background's contrast and brightness are to be ensured (Hargather and Settles 2012).

BOS is also able to factor in several light sources. To obtain informative images, the high contrast of the background and an appropriate sensitivity concerning small image shifting are of importance (Panigrahi and Muralidhar 2012).

The sensitivity of the system is defined as the smallest displayable deflection angle (Gojani et al. 2013). Here, the focal length and the aperture, the relative position of the measuring object between the camera and the background, as well as the smallest measurable pixels on the image plane are the main factors, which affect the sensitivity of the experiment. The smallest detectable shift of the structured background is determined by its quality and the evaluation methods. For the following investigations, cross-correlation algorithms were used for analysis. Alternatively, block-matching or optical flow algorithms can be used.

2.2. Experimental setup

The empirical investigations were implemented in the climate laboratory of the Department of Building Physics at the Bauhaus-University Weimar, Germany. The climate laboratory is a thermally-independent room with dimensions of approximately 3.00 × 3.00 × 2.40 m. Its surfaces can be heated separately for setting up an indoor climate without any disturbing air flow. The consistent experimental conditions enable the comparison of measurements over a long period of time.

As in a conventional BOS setup, the experimental setup for the two-dimensional evaluation consists of a structured background, the object under investigation, and a high-resolution camera that is located as far away as possible from the background. The schematic setup as well as a detail of the used structured background are shown in Fig. 2.

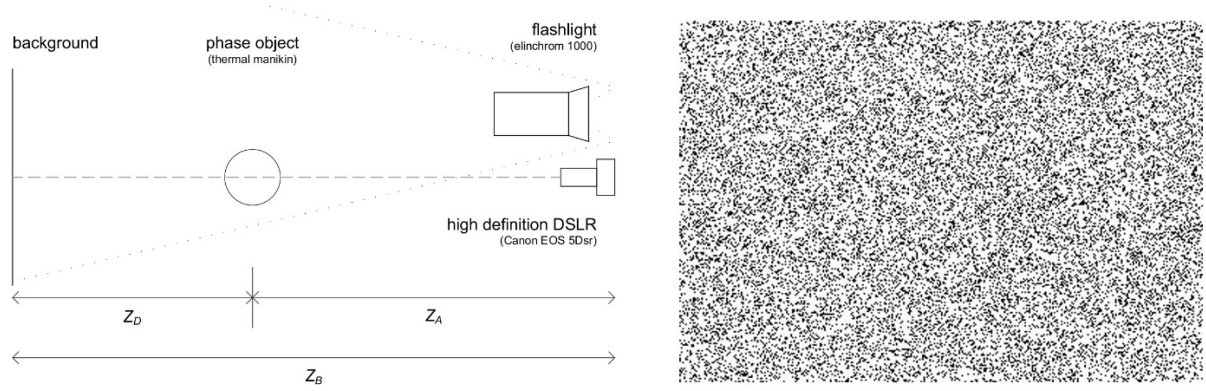

Fig. 2 *Schematic experimental setup (left) and detail of the structured background (right)*

The structured background was plotted on paper as to not impair the heatable walls of the laboratory. The structure was black pixels on a white surface with a total density of 25 %. Furthermore, the pixels show angular boundaries to increase the experiment's sensitivity. For better illumination, the room was lit by a flashlight, which illuminated the structured background indirectly. The dimension of the setup was Z_B = 250 cm.

The flow under investigation was a free convective flow caused by the heat release of a thermal manikin. The manikin consists of 22 heatable body segments to simulate the human heat emission (Voelker et al. 2014). The manikin was set to comfort mode, which simulates the skin temperature of an occupant in a calm state. This mode was chosen because it is widely used in studies that investigate the indoor environment (Alsaad and Voelker 2018). The manikin was left nude to simplify the measurements. Moreover, using a manikin wearing no clothes also results in higher convective flow velocities compared to a dressed manikin (Licina et al. 2014).

The flow was captured by a high-resolution full-frame DSLR camera *Canon EOS 5Dsr* with an effective resolution of approximately 50.6 megapixels. The lenses used were *ZEISS Milvus 2/135* with a fixed focal length f = 135 mm and *Sigma DG Macro HSM* with a fixed focal length f = 105 mm. Lenses that have variable focal lengths are not suitable because of the complex lens systems that cause geometric and radiometric aberrations leading to inaccurate measurements.

Regarding the aperture of the camera, the image's minimal diameter limited by diffraction is reduced if the recording is captured with a small $f_\#$-number (corresponds to a wide aperture). However, the geometrical noise increases, which results in a reduction of the depth of field. The background always has to be in focus to detect image shift. At the same time, sharp imaging of the investigated flow is of great importance to extract the specific features of the flow. To reduce this image noise and to increase the depth of field, the $f_\#$-number in the experimental setups is maintained at a high value. If the aperture is too small, rays will be diffracted and lead to blurred images. Small $f_\#$-numbers that lead to diffraction blur depend on the camera. The diffraction blur can be seen already at $f_\#$ = 8 with the camera used here. As the $f_\#$-number increases, so does the diffraction blur and the depth of field. Therefore, an appropriate aperture needs to be chosen. The diffraction blur also depends on the quality of the lens system. As the diffraction blur only affects the images slightly and a high depth of field is important, in this case, the camera setting $f_\#$ = 22 was chosen.

Additionally, to increase the sensitivity of the setup, it is recommended to use high focal lengths f. This is because of the camera's opening angle – when it decreases, presumably, parallel light reaches the camera sensor, hence, light rays can be assumed to be travelling in Gaussian optics. Here, the lens' opening angle of the camera Canon EOS 5Dsr is $\alpha \approx 24.6$ ° with f = 105 mm and $\alpha \approx 19.6$ ° with f = 135 mm. Furthermore, the ISO value of the camera needs to be as small as possible to minimize sensor noise. It is less important to minimize the exposure time t when it comes to investigating slow flow, such as convective flow. Yet it should not be greatly increased, which results in an average of the flow under investigation. Here, the camera's settings were kept constant at ISO 100 and exposure time t = 1/125 s. When working with such small apertures and low ISO values coercively, the background has to be illuminated well. Therefore, an *elinchrom 1000* flashlight with a gross luminosity of 1,000 Joule was installed. Furthermore, the images are saved in RAW format to enhance several settings, such as contrast, brightness, sharpness and noise without losing information of the image.

Fig. 3 shows the measurement setup in the climate laboratory for two-dimensional investigations of the convective flow. Omnidirectional hot-wire anemometers with an accuracy of ± 1.5% and NTC sensors with an accuracy of ±0.1 K were installed to measure the air velocity and the temperature. The anemometers were mounted at h = 6, 27, and 48 cm, the NTC sensors at h = 2, 23, and 44 cm above the manikin's crown.

Fig. 3 *Experimental setup in the climate laboratory with the thermal manikin, anemometers, and NTC sensors*

Fig. 4 shows the conventionally measured air temperatures and flow velocities. In the core of the thermal plume, velocities of up to 0.21 m/s were measured by anemometry. This is equivalent to a Reynolds number of around 2.23×10^3. The temperature difference between the thermal plume and the undisturbed room air near the manikin's head at h = 2 cm is $\Delta T \approx 4.1$ K. At h = 44 cm above the manikin's head, the temperature difference is $\Delta T \approx 1$ K, measured by the temperature sensors. Both, the temperatures and velocities of the density gradient are dependent on the height of the sensor and the time. The differences of the measured velocities vary widely due to the transient and turbulent properties of the flow. An exception is the sensor near to the boundary layer at h = 6 cm that lies within a "dead zone" (laminar flow directly above the manikin's head).

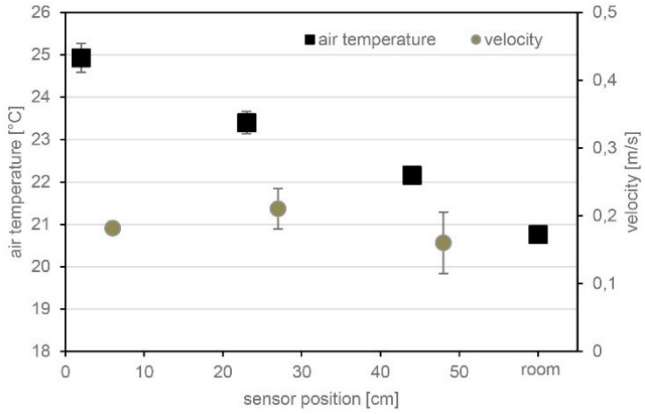

Fig. 4 *Air temperatures and velocities above the manikin's head*

Fig. 5 shows the virtual displacement Δy of the pixels on the background plane according to the refractive index gradients. With the help of the ideal gas law, the density ρ of the fluid can be calculated. Furthermore, the conventional measured air temperatures depicted in Fig. 4 can be used to calculate the refractive index n (Eqn. 1). Finally, with the help of the thin-lens approximation (Eqn. 5) and Eqn. 2, the displacement Δy can be roughly estimated.

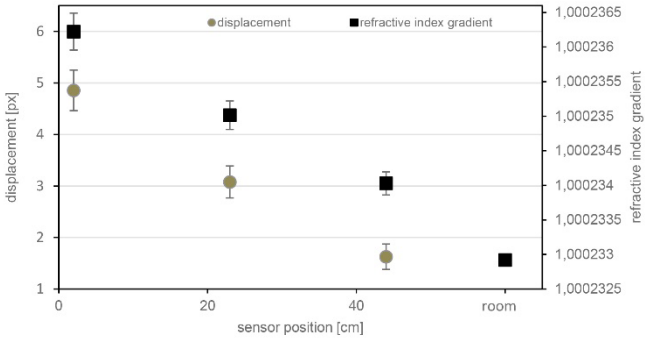

Fig. 5 *Displacement Δy and the corresponding refractive indices at Z_D = 100 cm and f = 105 mm*

2.3. Empirical investigations

To optimize the setup, 16 experiments (grouped in three test series) with varying parameters were conducted. Table 1 shows the different experiments with the dot diameter $\emptyset$ in mm, the distance between the phase object and the background Z_D in mm, the focal length f in mm, and the room air temperature Θ in °C. For analysis, an image with the heated thermal manikin (flow-on) was taken first followed by an image without the phase object (flow-off).

In the experiment series 1 and 2, three background structures with different dot diameters were used to determine which one is able to show the smallest virtual displacement. Structures with dot diameters of 0.42, 0.22, and 0.14 mm and 25 % pixel density each were investigated. Preliminary investigations showed that working with a pixel density of 25 % yields the highest sensitivity. Smaller densities result in a loss of information because less pixels can be tracked. Higher pixel densities also lose information due to the black dots overlapping when the light rays are deflected. Images were taken with f = 135 mm and f = 105 mm to detect any differences in the resolution of the evaluation. Additionally, different room temperatures resulting in different temperature gradients were investigated. Furthermore, various focal lengths were used to determine the influence on the evaluations. The sensitivity of the experimental setup exponentially increases when the focal length f increases. Although larger focal lengths yield a higher sensitivity of the experimental setup, a focal length f = 135 mm only shows little detail of the measuring field due to the spatial restriction of the climate laboratory. For that reason, further images were taken with f = 105 mm.

According to the finding in the previous experiment, dot diameters of 0.22 mm were set in experiment series 3. Here, distances between the phase object and the background were varied. As the distance from the phase object to the background Z_D increases, so does the sensitivity. Because the camera exclusively focuses on the background to detect image shifting, the refractive index gradient appears blurred as a result. The closer the density gradient is located to the background to depict it more sharply, though, the lower the setup's sensitivity will be (see Fig. 8). Thus the flow was visualized best in experiment series 3g when working with a distance Z_D = 1000 mm, using the settings described in the following section 2.4.

Experiment	a	b	c	d	e	f	g
1	$\emptyset$ = 0.14 Z_D = 950 f = 135 Θ = 22	$\emptyset$ = 0.22 Z_D = 950 f = 135 Θ = 22	$\emptyset$ = 0.42 Z_D = 950 f = 135 Θ = 22	$\emptyset$ = 0.14 Z_D = 950 f = 105 Θ = 22	$\emptyset$ = 0.22 Z_D = 950 f = 105 Θ = 22		
2	$\emptyset$ = 0.14 Z_D = 950 f = 105 Θ = 20	$\emptyset$ = 0.22 Z_D = 950 f = 105 Θ = 20	$\emptyset$ = 0.14 Z_D = 950 f = 135 Θ = 20	$\emptyset$ = 0.22 Z_D = 950 f = 135 Θ = 20			
3	$\emptyset$ = 0.22 Z_D = 400 f = 105 Θ = 20	$\emptyset$ = 0.22 Z_D = 500 f = 105 Θ = 20	$\emptyset$ = 0.22 Z_D = 600 f = 105 Θ = 20	$\emptyset$ = 0.22 Z_D = 700 f = 105 Θ = 20	$\emptyset$ = 0.22 Z_D = 800 f = 105 Θ = 20	$\emptyset$ = 0.22 Z_D = 900 f = 105 Θ = 20	$\emptyset$ = 0.22 Z_D = 1000 f = 105 Θ = 20

Table 1 *Experiments and the corresponding parameters*

2.4. Analysis

To emphasize the contrast and sharpness of the background as well to reduce chromatic aberrations and vignetting, the images were pre-processed in appropriate photo-editing applications before analysis (here: *DxO PhotoLab*).

For two-dimensional evaluation of the air flow, the application *PIVview2C* was used, developed by the German Aerospace Center (DLR). This application uses cross-correlation algorithms to detect pixel shifts between two images by comparing the intensity distribution of the brightness of both, the reference as well as the measuring image (Raffel 2002).

The displacement vector Δy between the reference and the measuring image describes the deflection angle ε_y of any light ray passing the field of view. To calculate the image displacement *Δy*, PIVview2C uses image deformation schemes (window deformation) under the assumption that the motion of the pixels within each interrogation window is approximately uniform. For evaluation, the following equation is used:

$$R_{\mathrm{II}}(x,y) = \sum_{i=-K}^{K} \sum_{j=-L}^{L} \tilde{I}(i,j)\, \tilde{I}'(i+x, j+y) \tag{6}$$

Here, $\tilde{I}(i,j)$ and $\tilde{I}'(i,j)$ are the image intensities reconstructed after deformation using the predicted deformation field $\Delta s(x)$ in a central difference scheme:

$$\tilde{I}(x) = I\,(\boldsymbol{x} - \frac{\Delta \boldsymbol{s}(\boldsymbol{x})}{2}) \tag{7}$$

$$\tilde{I}'(x) = I'(\boldsymbol{x} + \frac{\Delta \boldsymbol{s}(\boldsymbol{x})}{2}) \tag{8}$$

The deformation field $\Delta s(x)$ requires interpolation at each pixel. This is due to $\Delta s(x)$ being a spatial distribution that generally is not uniform (Raffel et al. 2018).

For the purpose of investigating slow convective flows while using background patterns with small structures, the interrogation window can be kept small. However, if the window size becomes too small errors can accumulate more easily. Therefore, it is necessary to adjust the interrogation window size to the experimental conditions. Furthermore, the windows will be overlapped to minimize data loss that results from pixels shifted out of frame. Here, the optimal overlap is 50 %, a window size of 24 pixels, and a step size of 12 pixels. If the overlap is increased, more data will be produced, which does not necessarily lead to additional information. The multi-grid interrogation was used as well as the sub-pixel image sifting to detect displacements that are smaller than one pixel. To avoid irritations of the analysis algorithms, disturbing elements (such as the measurement object or the measuring instruments) are masked (values are equal to zero).

Due to uncertainties resulting from many factors such as the camera settings or the analyzing algorithm, noise cannot be eliminated completely in the results. To avoid the appearance of noise as much as possible, low ISO values and small apertures were used, which both have the highest impact on noise. Since the experimental setup and the definition of the parameters of the analyzing algorithm were conducted precisely and concisely, there was no large noise to detect. Small movements of the printed background pattern could occur due to the structure being taped to the walls of the climate laboratory. However, any movement was avoided as much as possible.

Due to the high-resolution DLSR camera Canon EOS 5Dsr, the image size of the uncompressed files is about 150 megabyte per frame. Using standard computational conditions (8 gigabyte RAM and 3 gigahertz processor), each image pair takes about 50 seconds to process. In this case, the execution time only varies slightly with respect to the image size. Using PIVview2C for evaluation offers the possibility to extract the mean vector of each interrogation window. Calibrating the lengths of the images allows for extracting the displacement for each mean vector. Nogueira et al. (2005) show that it is possible to detect displacements of 0.1 pixels using cross-correlation algorithms. When analyzing the images using the algorithm and its settings described above, it is possible to detect pixel shifting of 1.4 pixels, which is a virtual displacement of approximately 8 µm on the background plane.

3. Results

Fig. 6 - 8 show the results, which were analyzed based on the method described in section 2.4. The turbulent structure in the results above the scalp of the manikin's head (blue semicircle at the bottom of the images) is the convection due to the heat release of the manikin. The structures of the

flow show the displacement of the pixels in x- and y- direction (refractive index gradients dn/dx and dn/dy). Fig. 6 shows the results of experiment series 1 a - c according to Table 1. In this experiment, the following parameters were set: distance Z_D = 950 mm, room air temperature Θ = 22 °C, and focal length f = 135 mm. The pixel diameter of the structured background was varied between 0.42, 0.22, and 0.14 mm. Below each analysis, the actual dot size of a single pixel is shown.

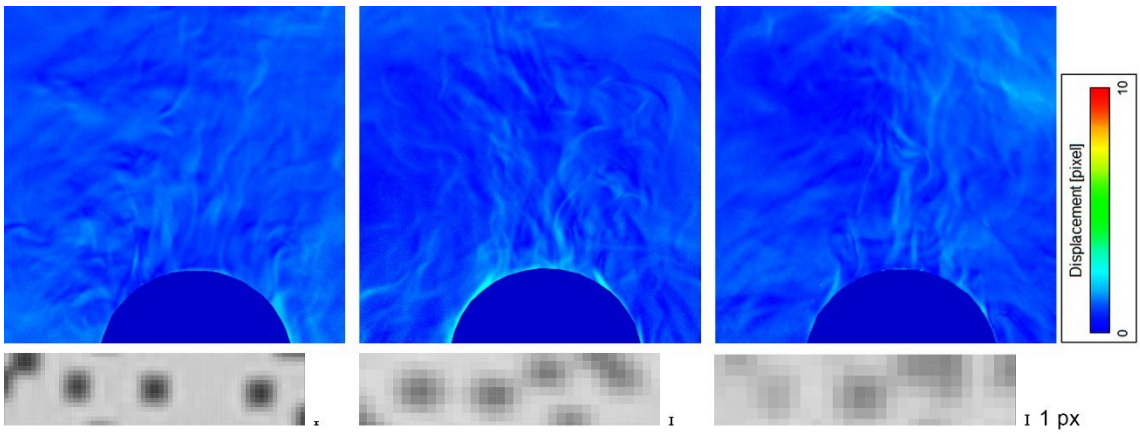

Fig. 6 *Results with Ø = 0.42 mm (left), Ø = 0.22 mm (center), and Ø = 0.14 mm (right)*

Theoretically, the optimal dot diameter is reached if one dot is displayed on approximately 3-5 pixels on the camera sensor. Smaller diameters between 2-3 pixels would increase the sensitivity of the measurement but usually, this cannot be achieved due to diffraction-limited imaging at high $f_\#$-numbers and the small pixel pitch of current cameras (Raffel 2015).

Based on the analysis, the best results can be achieved with a dot diameter of 0.22 mm. One dot has an approximate size of 9 pixels on the camera sensor, see Fig. 6 (center). If the diameter decreases to 0.14 mm, the dots cannot be captured with sufficient contrast and sharpness despite theoretical considerations. Increasing the diameter to 0.42 mm also leads to a lower resolution of the results because fewer pixels can be tracked.

Furthermore, the flow can be visualized more easily if the temperature difference between the thermal manikin and the room air and, therefore, the density gradient increases. This means that the deflection of the rays is larger due to the greater refractive index gradient. Hence, the room air temperature was set to Θ = 20 °C in the following experiments.

Fig. 7 shows the results of the investigations using various focal lengths f = 105 mm and f = 135 mm. Here, the following parameters were set: Z_D = 950 mm, room air temperature Θ = 20 °C, and dot diameter Ø = 0.22 mm according to Table 1 experiment series 2 b and d. Although larger focal lengths yield a higher sensitivity of the BOS system, f = 105 mm was used for further investigations due to the restricted spatial dimensions of the climate laboratory.

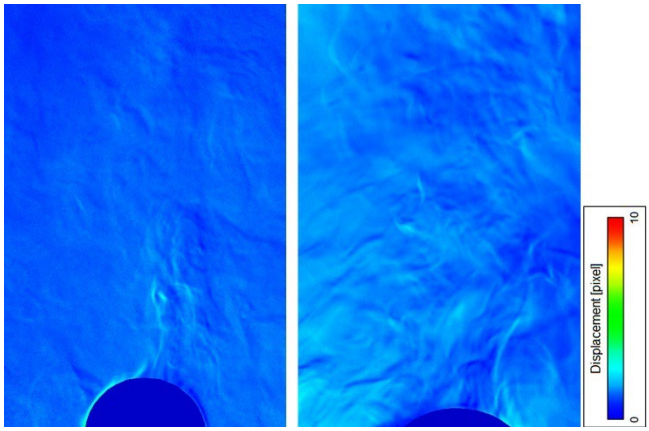

Fig. 7 *Results at f = 105 mm (left) and f = 135 mm (right)*

In experiment series 3, the following parameters were set: dot diameter Ø = 0.22 mm, room temperature Θ = 20 °C, and focal length f = 105 mm.

To determine the optimal distance between the phase object and the background, Z_D was varied between 40 cm and 100 cm with step sizes of 10 cm. Fig. 8 exemplary shows results at Z_D = 40 cm, Z_D = 70 cm, and Z_D = 100 cm.

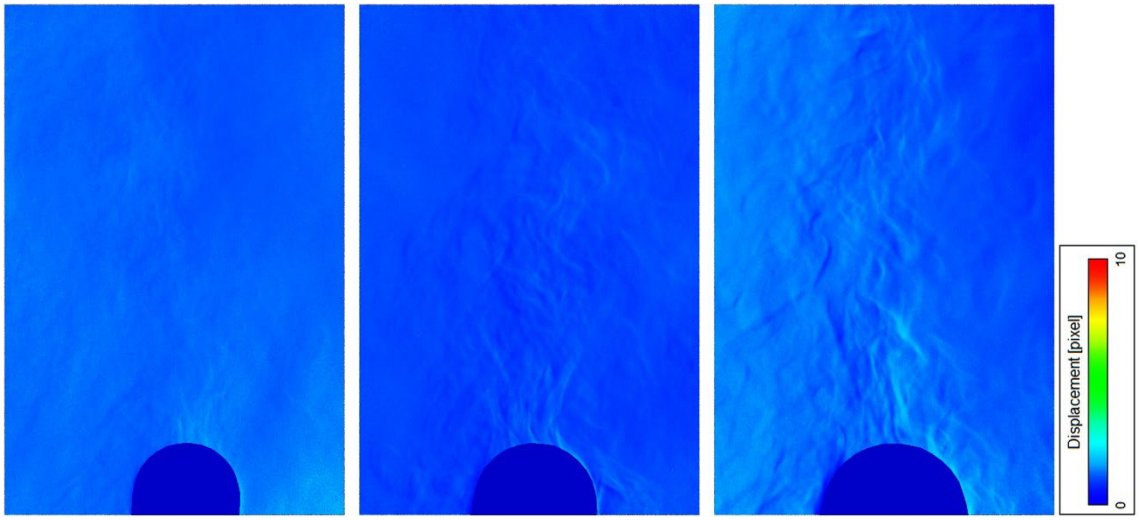

Fig. 8 *Results at Z_D = 40 cm (left), Z_D = 70 cm (center), and Z_D = 100 cm (right)*

It can be seen that the lowest resolution of the system is at Z_D = 40 cm even if the investigated flow appears to be the sharpest because of the small distance between the phase object and the background. At Z_D = 70 cm, the flow can be perceived clearly. However, the pixel shifting is not as high as it appears at Z_D = 100 cm. Here, large image shifting can be detected both within the boundary layer and high above the phase object. This is due to the light ray travelling continuously through the homogeneous room air after its deflection and therefore enlarging the virtual displacement. The flow field appears slightly blurred, though, due to the large distance between the background and the density gradient. Accordingly, an optimal distance Z_D can be regarded as Z_D = 100 cm for the chosen circumstances. This means that when choosing a suitable distance, attention has to be paid either to the sharpness of the flow field or the sensitivity of the setup.

The results in Fig. 8 indicate that the evolved system presented in this article is able to detect least density gradients with temperature differences $\Delta T < 1$ K. As this small temperature gradient is clearly visible, the chosen setup and its sensitivity is able to visualize and measure convective indoor air flows.

4. Conclusions

The advantage of any schlieren technique is to measure density gradients without disturbing the flow field. These techniques produce qualitative results only in the form of a two-dimensional projection due to the integration along a line of sight. To obtain quantitative results that are not line-integrated, it is necessary to use stereoscopic or tomographic setups, e.g. by capturing the flow field with more than one camera. Appropriate algorithms (e.g. filtered back projection, algebraic reconstruction technique) then can be used to reconstruct the field of view three-dimensionally.

The simple setup, the almost unlimited size of the measurement field, and the relative ease of measurements are significant advantages of the BOS technique. In this paper, a BOS setup is presented that is able to visualize very small temperature gradients resulting from the thermal plume above a thermal manikin due to natural convection. These density gradients in transparent media can be visualized with the help of only a small number of tools. The apparent deformation of the background structure due to an inhomogeneous density field allows for the visualization of the flow in detail. For determining the velocity of a fluid along a line of sight in the case of natural convection, it is necessary to add an adjustment factor to compensate for the distance Z_D between the structured background and the phase object, which is not a fixed value for every setup. For an increasing distance Z_D, the image displacement Δy will increase too due to the light ray travelling continuously between the phase object and the background pattern and therefore enlarging the virtual displacement. For extracting the velocity out of density, the Navier-Stokes equations show the relation between them.

The object under investigation always appears blurred because the camera only focuses on the background to detect image shifting. To obtain desired results (higher level of detail vs. higher level of accuracy), it is important to weigh the appropriate parameters. Furthermore, the level of detail can be increased when minimizing the dot diameter until it covers 3-5 pixels of the camera sensor. Therefore, the quality and resolution of the structured background are significant to obtain results of high quality. If the dot size decreases, the parameters of the setup, as well as the illumination and high contrast of the background have to be ensured. Conversely, this also means that large density gradients can be displayed under adverse conditions.

The spatial dimensions of the setup do not affect the sensitivity or accuracy of the results. Rather, modifiable parameters, such as the camera's resolution and the background structure, need to have a sufficient quality, as required by the experimental conditions. Considering these requirements, BOS is able to visualize small density gradients. After varying the parameters that define the sensitivity of the setup, the BOS technique presented in this article is able to display temperature differences of $\Delta T < 1$ K and a resulting image shift of approximately 8 µm. It should be noted that this

value only represents an integration of single values that are in a line of sight for each specific light ray. The findings discussed in this paper contribute to understanding the properties of large-scale indoor air flows and are promising for future measurements of indoor air flows.

Acknowledgements

The authors would like to thank the contributions of M. Spreer, J. Brooks and L. Martin for their help and support.

References

Alsaad H, Voelker C (2018) Performance assessment of a ductless personalized ventilation system using a validated CFD model. Journal of Building Performance Simulation 11:689–704. https://doi.org/10.1080/19401493.2018.1431806

Gardner AD, Raffel M, Schwarz C, Braukmann JN, Wolf CC (2020) Reference-free digital shadowgraphy using a moving BOS background. Exp Fluids 61. https://doi.org/10.1007/s00348-019-2865-4

Gena AW, Voelker C, Settles GS (2020) Qualitative and quantitative schlieren optical measurement of the human thermal plume. Indoor Air. https://doi.org/10.1111/ina.12674

Gojani AB, Kamishi B, Obayashi S (2013) Measurement sensitivity and resolution for background oriented schlieren during image recording. Journal of Visualization 16:201–207. https://doi.org/10.1007/s12650-013-0170-5

Goldhahn E (2009) Weiterentwicklung der Hintergrundschlierenmethode zu einem quantitativen Verfahren der Vermessung von Dichtefeldern: Dissertation. Leibniz University Hannover (Germany)

Hargather MJ, Settles GS (2012) A comparison of three quantitative schlieren techniques. Optics and Lasers in Engineering 50:8–17. https://doi.org/10.1016/j.optlaseng.2011.05.012

Keagy WR, Ellis HH (1948) The application of the schlieren method to the quantitative measurement of mixing gases in jets. Symposium on Combustion and Flame, and Explosion Phenomena 3:667–674. https://doi.org/10.1016/S1062-2896(49)80092-4

Licina D, Pantelic J, Melikov A, Sekhar C, Tham KW (2014) Experimental investigation of the human convective boundary layer in a quiescent indoor environment. Building and Environment 75:79–91. https://doi.org/10.1016/j.buildenv.2014.01.016

Mazumdar A (2013) Principles and Techniques of Schlieren Imaging Systems. Columbia University Computer Science Technical Reports. https://doi.org/10.7916/D8TX3PWV

Nogueira J, Lecuona A, Rodrìguez PA (2005) Limits of the resolution of correlation PIV iterative methods. Fundamentals. Experiments in Fluids 39:305–313. https://doi.org/10.1007/s00348-005-1016-2

Panigrahi PK, Muralidhar K (2012) Schlieren and Shadowgraph Methods in Heat and Mass Transfer. Springer New York, New York, NY

Raffel M (2002) Optische Untersuchungen in technischen Strömungen unter besonderer Berücksichtigung eines Verfahrens zur Detektion von Dichtegradienten. Zugl.: Clausthal, Techn. Univ., Habil.-Schr., 2001, 1. Aufl. Papierflieger, Clausthal-Zellerfeld

Raffel M (2015) Background-oriented schlieren (BOS) techniques. Experiments in Fluids 56:60. https://doi.org/10.1007/s00348-015-1927-5

Raffel M, Willert CE, Scarano F, Kaehler CJ, Wereley ST, Kompenhans J (2018) Particle image velocimetry: A practical guide / by Markus Raffel, Christian E. Willert, Fulvio Scarano, Christian J. Kaehler, Steve T. Wereley, Juergen Kompenhans. Springer, Cham

Rajshekhar G, Ambrosini D (2018) Multi-scale approach for analyzing convective heat transfer flow in background-oriented Schlieren technique. Optics and Lasers in Engineering 110:415–419. https://doi.org/10.1016/j.optlaseng.2018.07.002

Ramaiah J, Ajithaprasad S, Gannavarpu R, Ambrosini D (2020) Fast and robust method for flow analysis using GPU assisted diffractive optical element based background oriented schlieren (BOS). Optics and Lasers in Engineering 126:105908. https://doi.org/10.1016/j.optlaseng.2019.105908

Settles GS (2001) Schlieren and Shadowgraph Techniques: Visualizing Phenomena in Transparent Media. Springer-Verlag Berlin Heidelberg, Berlin Heidelberg

Settles GS (2010) Important developments in schlieren and shadowgraph visualization during the last decade. Proceedings of 14th International Symposium on Flow Visualization, Daegu (Korea):267

Voelker C, Maempel S, Kornadt O (2014) Measuring the human body's microclimate using a thermal manikin. Indoor Air 24:567–579. https://doi.org/10.1111/ina.12112